Optimization of multilayer reflectors for extreme ultraviolet lithography

Matthieu F. Bal
Mandeep Singh
Joseph J. M. Braat
Delft University of Technology
Optics Research Group
Faculty of Applied Sciences
Lorentzweg 1
2628 CJ Delft
The Netherlands

Abstract. Multilayer interference coatings on reflective elements in extreme ultraviolet (EUV) projection lithography systems introduce phase and amplitude variations at reflection, which have important implications for imaging properties, e.g., resolution, depth of focus, and tolerances. We discuss the numerical results of the optical effects of multilayers (MLs) and the inclusion of these effects in optical design. This numerical study demonstrates the advantages of spatially varying (graded) MLs compared to multilayers with constant layer thicknesses. We present a new method to calculate the optimum grading of multilayers. Using this new method, we are able to fully optimize the wavefronts emerging from the projection system toward the image plane. [DOI: 10.1117/1.1793171]

Subject terms: multilayer; optimization; extreme ultraviolet lithography; graded multilayers; imaging.

Paper 03073 received Oct. 16, 2003; revised manuscript received Mar. 30, 2004; accepted for publication May 19, 2004.

1 Introduction

The next generations of lithographic systems aim to image patterns with features smaller than 45 nm. A likely candidate for volume production of integrated circuits is extreme ultraviolet (EUV) lithography, which is an extension of optical lithography techniques into EUV wavelengths.[1] These systems must consist of reflective optics, since the EUV illuminating radiation (typically in the 11- to 16-nm spectral region) is highly absorbed in all materials. Despite this absorption, a relatively high reflectivity is obtained with the aid of multilayer (ML) deposition.[2] Typically, in the 11- to 16-nm spectral region, these types of MLs consist of alternating layers of molybdenum and silicon (or molybdenum and beryllium), and are now fabricated routinely with reflectivity close to the theoretical limit ($\sim$70%).[3]

The optical performance of EUV projection systems is modeled, evaluated, and optimized with the aid of optical design programs.[4,5] The influence of the MLs on reflecting properties can be neglected in the early design stages. Throughout these stages, a ML can be represented by a perfectly reflecting single surface. Once the projection system reaches the diffraction limit, the effect of the MLs must be included. The imaging properties of the projection system (e.g., resolution, depth of focus, and tolerances) are considerably affected by the phase and amplitude variations produced by standard MLs. We present and apply a design criterion that assures the optimum adaptation of the multilayer structures (grading) to the imaging requirements of the EUV projection system.

2 Modeling of Multilayers in Optical Design

In the first stages of the optimization of an optical system with MLs, the phase and intensity variations induced by MLs are ignored and the surface is replaced by a single perfectly reflecting surface. In the case of reflection at a single interface between two different media, the reflectivity and phase shift depend on the complex refractive indices n of the two media and the angle of incidence θ. The origin of the reflected ray is the point of intersection of the incident ray with the interface. The direction of the reflected ray is determined by the fact that the angle of reflection is equal to the angle of incidence.

In a later stage of optimization, the effects of MLs must be taken into account. The reflectivity and the phase shift of a ray reflected from a ML now strongly depend on the angle of incidence θ and the thicknesses and refractive indices of the materials in the ML. The differences in phase shift of rays reflecting at a ML have to be included when evaluating the imaging quality of a projection system. Liang et al.[6] analytically looked at the aberrations introduced by ML coatings on a tilted flat mirror in the case of an obliquely incident finite aperture beam. They found, up to second-order aberrations, a first-order field-dependent piston, a field-squared piston, defocus, field-independent tilt, field-independent astigmatism, and anamorphic magnification. Duddles[7] found that wave aberrations introduced by ML incorporation in EUV projection systems can be effectively described by a simple tilt and defocus of the wavefront, allowing system performance to be recovered to a level close to that of the bare system. Cerrina et al.[8] report a non-negligible amount of spherical aberration introduced by the MLs and a change of apparent focal length of the optics.

When performing thin-film calculations, one assumes an infinitely extending plane wave incident on a ML consisting of plane parallel surfaces. The calculations coherently sum all reflections coming from the different transitions in the MLs. These thin-film calculations are based on standard matrix methods.[9] The total reflected field depends on the geometry of the normal $\mathbf{v}$ to the ML surface and the wave vector $\mathbf{k}$. In the case of 2-D ML structures, the superposi-

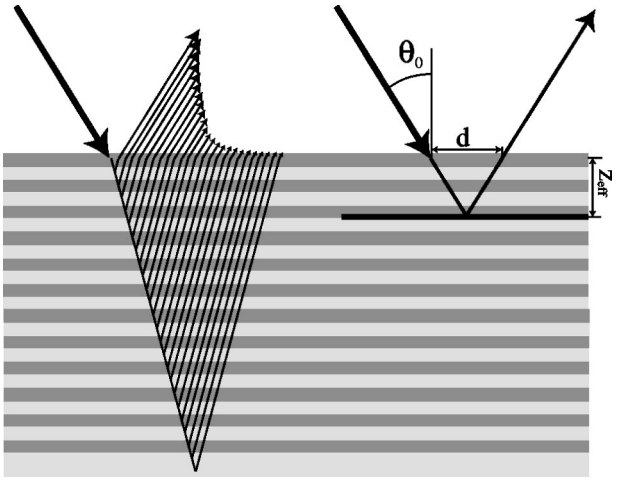

Fig. 1 Two approaches for representing the field reflected by a ML structure. On the left-hand side, the approximation of reflected fields results in a large collection of rays with different phases and lateral displacements. On the right-hand side, the average reflected field has a lateral displacement *d* and reflects at the effective reflection depth z_{eff} in vacuum.

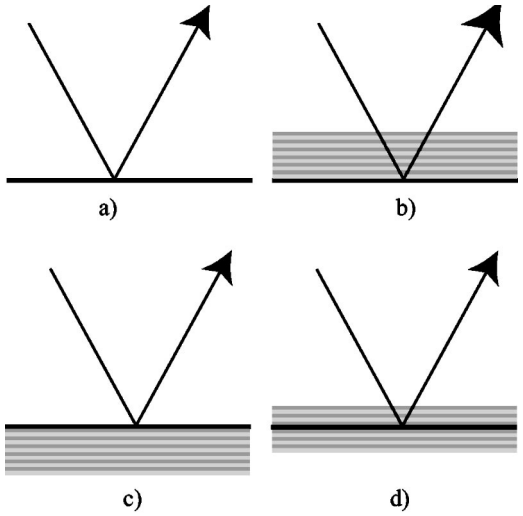

Fig. 2 Various ways to include MLs on a reflective surface. (a) The surface is a single transition between two media. (b) The substrate is the original surface. The method in (c) produces smaller alterations to the characteristics of the EUV projection systems, as the thickness of the ML stack is many times the wavelength. In (d), the effective reflection depth represents the average location of the reflections and coincides with the original single transition.

tion of the infinite series of reflected (or transmitted) waves can be represented by a single plane wave with a certain phase φ, measured with respect to the top surface of the ML (see Fig. 1). The input field E_i is related to the reflected field E_r by

$$E_r = |r(\mathbf{k},\mathbf{v})| E_0 \exp[i\phi(\mathbf{k},\mathbf{v})], \tag{1}$$

where the absolute value of r is the relative amplitude. The reflection coefficient $|r|$ is defined as

$$|r| = \left| \frac{E_r}{E_0} \right|. \tag{2}$$

Of course, both the reflection coefficient r and the phase φ depend on the state of polarization of the incident field. Using thin-film calculations, for instance via an optical design program or a separate thin-film[10] program, one computes the phase shift, modulo 2π, and the amplitude of the reflected field as a function of the location of the point of incidence, the angle of incidence, the wavelength, and the state of polarization. Different alternatives exist to locate the ML when replacing the single transition by the multilayer structure. These are discussed next.

1. Normally, ML coatings are employed for reflection enhancement, antireflection, bandpass filters, edge filters, or other complex functions of intensity versus wavelength. In many of these situations, the reference surface is chosen to be the substrate-ML interface [see Fig. 2(b)]. This approach becomes less appropriate for MLs with a total thickness much greater than a wavelength, as in the case of EUV MLs.
2. An alternative approach is to have the top of the ML coincide with the original surface [see Fig. 2(c)]. The largest contribution to the reflected field comes from the upper part of the ML, since the materials in an EUV ML are absorptive.
3. In our analysis, we make the so-called effective reflection depth z_{eff} coincide with the original single transition surface [see Fig. 1 and Fig. 2(d)]. The effective reflection depth is a fictitious surface and defines the interface between vacuum and an imaginary substrate with a complex refractive index that is derived from the ML admittance.[9] This location minimizes the difference between an optical system modeled with and without MLs. Another advantage is that we include the lateral displacement, i.e., the distance on the top surface between the intersection points for the incoming and outgoing ray, as shown in Fig. 1.

Different methods exist to calculate the location of the effective reflection surface. Next, we discuss four numerical methods.

In the first method, the field reflected by a ML relates to the input field by a relative amplitude and a phase whose value we know up to a modulo 2π uncertainty [see Eq. (1)]. If we introduce an effective reflecting surface for the ML at a depth z_{eff} (in vacuum) below the top of the surface, the delay incurred by the incident composite wave is proportional to the extra traversed optical path. For the relation between the phase change on reflection φ of the output field and the effective reflection depth, we use the concept of group velocity, applied to the ML itself and to its geometrical equivalent, with an effective reflecting layer at a position z_{eff}. Using Fig. 1, the right-hand picture, we note for the optical phase difference in reflection over the depth z_{eff} in vacuum:

$$\varphi = 2z_{\text{eff}}(\mathbf{k}\cdot\mathbf{v}) = 2kz_{\text{eff}}\cos(\theta_0), \tag{3}$$

where $\cos(\theta_0) = \mathbf{k}\cdot\mathbf{v}/|\mathbf{k}|$. We define the angle of incidence θ

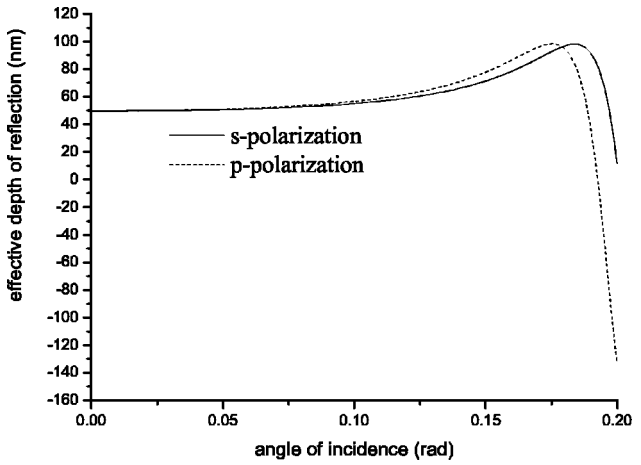

Fig. 3 The effective depth of reflection for both *s* and *p* polarizations from a ML consisting of molybdenum and silicon calculated with the first method.

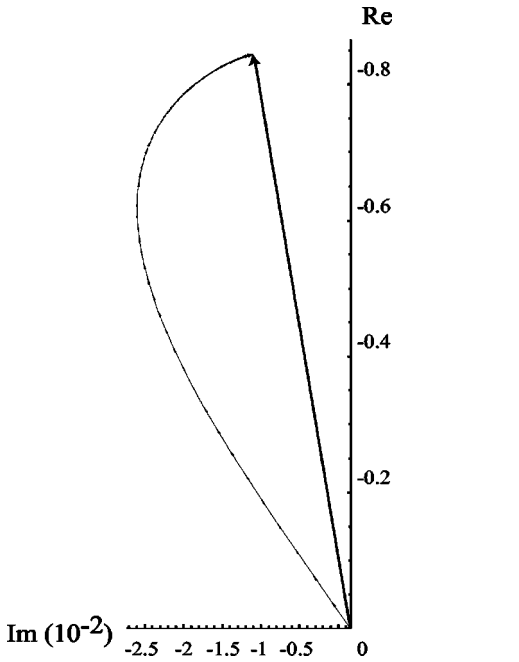

Fig. 4 The reflected field *r* plotted in the Gaussian plane. The phasors represent the difference in the complex reflectivity *r* between a ML with $j+1$ layers and *j* layers, where the additional layer has been added between the substrate and the ML. The sum of the phasors gives the total reflectivity of a Mo/Si ML of 50 periods.

as the angle between the wave vector **k** and the normal to the surface **v**. If we do not know the absolute phase, we can evaluate the derivative

$$\frac{\partial}{\partial|\mathbf{k}|}\varphi(\mathbf{k},\mathbf{v})=2z_{\mathrm{eff}}\cos(\theta_0). \tag{4}$$

The equivalent depth z_{eff} for a general multilayer now is obtained by calculating the quantity $\partial\varphi/\partial k$ for this multilayer at the central wave number in vacuum, $k=k_0$. The evolution of the effective depth of reflection calculated with Eq. (4) as a function of the angle of incidence is shown in Fig. 3.

Alternatively, we can also evaluate the value of $\partial^2\varphi/\partial\theta^2$ at the desired angle of incidence $\theta=\theta_0$. We can consider the equivalent depth z_{eff} independent of the angle of incidence θ_0 at near-normal incidence angles

$$z_{\mathrm{eff}}=-\frac{1}{2k_0\cos\theta_0}\frac{\partial^2\varphi}{\partial\theta^2}. \tag{5}$$

At near-normal incidence angles ($\theta_0=0$), we obtain z_{eff} from the expression

$$z_{\mathrm{eff}}=-\frac{1}{2k_0}\frac{\partial^2\varphi}{\partial\theta^2}=-\frac{1}{2k_0}\frac{\varphi(\theta+\epsilon)+\varphi(\theta-\epsilon)-2\varphi(\theta)}{\epsilon^2}, \tag{6}$$

where ϵ is an infinitesimally small number used to calculate the second-order derivative. As in Eq. (4), we can use the modulo-2π phase resulting from the thin-film calculations to calculate the effective reflection depth z_{eff} and/or the unwrapped phase shift. The approximation of the cosine of the angle of incidence makes Eq. (6) only valid for small incidence angles. At normal incidence, the effective depth calculated with Eq. (6) is approximately 50 nm.

In the third method proposed by Suematsu, Arai, and Kishino[11] and later elaborated on by Brovelli and Keller,[12] the latter use coupled-mode equations and Eq. (4) to come to an estimate of the effective depth of reflection of an infinitely thick perfect Bragg reflector at normal incidence. From the analysis in their work, we get an effective depth of reflection of 45 nm. It should be noted that in the Bragg reflector considered, there exists negligible absorption, unlike in the case of EUV reflectors. It is not entirely clear to us how valid an approach this is for EUV reflectors.

As a fourth method, we propose an approach utilizing the weighted average of the depth of all interfaces and abandon the local summation principle at the top of the multilayer. The separate axially and laterally displaced waves reflect from the ML structure, and we add the waves in the image plane. A complication here is the infinite number of waves that formally occur after reflection at the ML structure. We propose to simplify this picture by concentrating on the penetration depth of the first-order reflected waves. The contribution to the amplitude reflectivity D_j of layer *j* in a stack of layers can be approximated by

$$D_j=r_j-r_{j-1}. \tag{7}$$

The contributions of all transitions in a ML are a complex number and are represented by a vector (phasor) in Fig. 4. The difference in the reflected field of a ML with *j* and $j-1$ layers represents the contribution of layer *j*, originating at depth level z_j. All these differential contributions add up to the total reflectivity of a ML. We define the relative contribution of a transition w_j to the total reflectivity as the inner product of the differential reflectivity and the total reflectivity of the entire ML

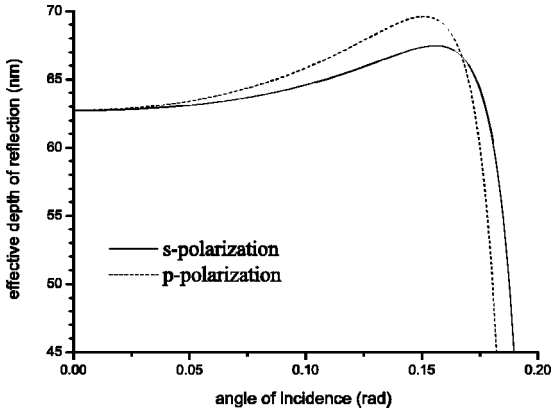

Fig. 5 The effective depth of reflection from a ML consisting of molybdenum and silicon obtained from the fourth method as a function of the angle of incidence.

$$w_j = \frac{\begin{bmatrix} \mathrm{Re}(D_j) \\ \mathrm{Im}(D_j) \end{bmatrix}^T \cdot \begin{bmatrix} \mathrm{Re}(r_t) \\ \mathrm{Im}(r_t) \end{bmatrix}}{|r_t|^2} = \frac{\mathrm{Re}(D_j r_t^*)}{r_t r_t^*}. \tag{8}$$

The summation of Eq. (8) over all transitions between media in the ML is unity. The relative contribution can be used as the weighting factor w_j in the calculation of the average depth of reflection and the average lateral displacement. The weighted average of the depth of all interfaces leads to the effective depth of reflection of a ML (see Fig. 5)

$$z_{\mathrm{eff}} = \sum_j w_j z_j, \tag{9}$$

where the quantity z_j denotes the optical distance between the top of the ML to the transition with number j. This method predicts a less sensitive dependence of the effective depth of reflection on the angle of incidence than the previous method. The evolution of the effective reflection plane as a function of the number of periods of a Mo/Si ML at normal incidence is presented in Fig. 6. The effective

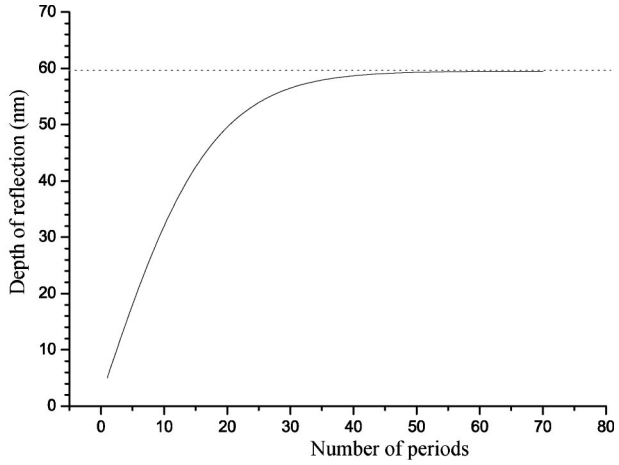

Fig. 6 The evolution of the penetration depth of a reflected field as a function of the number of periods of the ML. The horizontal dotted line indicates the saturation value of the effective depth of reflection.

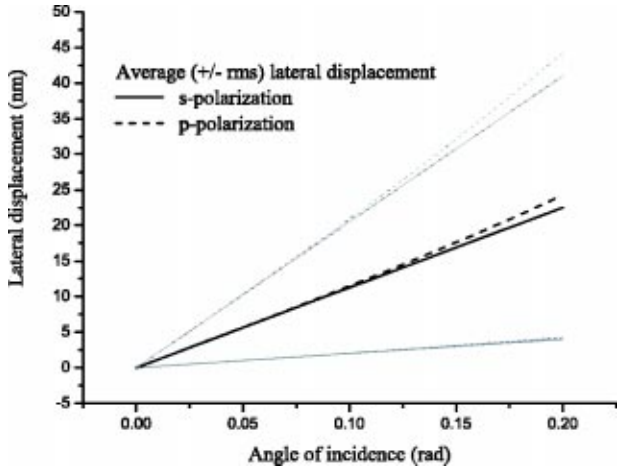

Fig. 7 The lateral displacement of rays incident on a ML are strongly dependent on the angle of incidence. In this example (black is the average, gray is the rms values), the dependence is almost linear with a gradient of 115 nm/rad.

reflection depth approaches a saturation value at around 45 to 50 periods; the reflected intensity reaches saturation with less periods (approximately 40 periods). Increasing the number of periods after the point of saturation does not change the phase of the reflected field. This property can, together with the fact that the reflectivity is saturated, be used in a correction method for ML or substrate height errors, as has been pointed out by Singh, Bal, and Braat.[13]

Another advantage of using the effective reflection plane is that we approximate the lateral displacement correctly with the average lateral displacement d. This average lateral displacement can easily be derived from the effective depth of reflection. A characteristic quantity for the lateral spread of the reflected beam (that is, the accuracy of the approximation) is the rms lateral displacement d_{rms}, defined by

$$d_{\mathrm{rms}} = \left[\frac{\Sigma_j w_j (z_j - z_{\mathrm{eff}})^2 \tan^2 \theta}{\Sigma_j w_j} \right]^{1/2}. \tag{10}$$

As shown in Fig. 7, the (rms) lateral displacement of the rays quickly increases at larger incidence angles.

3 Optical Performance of Systems with Multilayers

The complex amplitude change induced by a ML is a function of the angle of incidence and the thicknesses of the layers. The change in phase introduces a change of the reflected wavefront and a corresponding shift in ray direction (see Fig. 8). These changes are not considered in the approaches discussed so far. The presence of MLs is only manifested in the optical path length and the intensity of rays in optical design programs. Therefore, the rays could become oblique to the wavefront, which conflicts with the definition of a ray. This effect increases with increasing average angle of incidence (see Fig. 9). Another difficulty is that the thin-film calculations assume a plane wavefront incident on a plane surface with parallel MLs, while our systems have curved wavefronts and curved surfaces with graded MLs. The validity of the thin-film approximation in these situations is not indisputable.

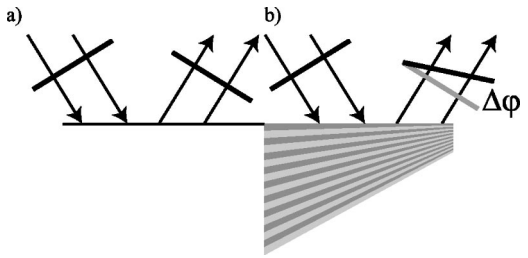

Fig. 8 The phase change originating from MLs depends among others on the angle of incidence and the thicknesses of the layers. Two rays, representing a plane wavefront, reflect at (a) a single transition or at (b) a graded ML. The phase variation originating from the ML is not equal for all rays in situation (b); consequently, there is no unique ray-wavefront combination in the reflected field. These types of layers demand a more thorough computation of the field resultant from the ML.

In the thin-film approximation, the summation of the partial fields reflected at any of the transitions is taken as the reflected field. One approach could be to consider all the fields reflected by the sequence of transitions separately. In an optical design program, a ray can normally not be split into a number of rays. The increase of the number of rays to evaluate would quickly lead to an intractable problem in the case of a large number of layers in the MLs, even when multiple reflections are neglected. In a six-mirror system with MLs consisting of 50 periods, each ray in the object plane would lead to $100^6 = 10^{12}$ rays in the image plane.

We therefore proceed along another path. To determine the effects of MLs on the optical properties of a system, we compare the point spread functions (PSFs) of a perfectly focused beam returning from a reflecting surface consisting of a single transition, and an assembly of beams reflected by a nongraded ML. In this example, a collimated beam is brought to a focus by a parabolic reflector, as shown in Fig. 10. The intensity of the point spread function of a single reflecting surface in a system with a numerical aperture (NA) of 0.3 in the image plane is shown on the left-hand side in Fig. 11.

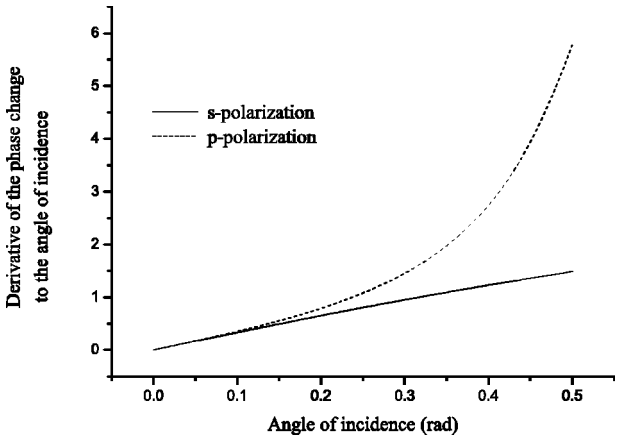

Fig. 9 The derivative of the phase change with respect to the angle of incidence demonstrates an increasing effect at larger average angles of incidence. The layer thicknesses of the ML are adjusted to the average cosine of the angle of incidence (horizontal axis) using Eq. (11).

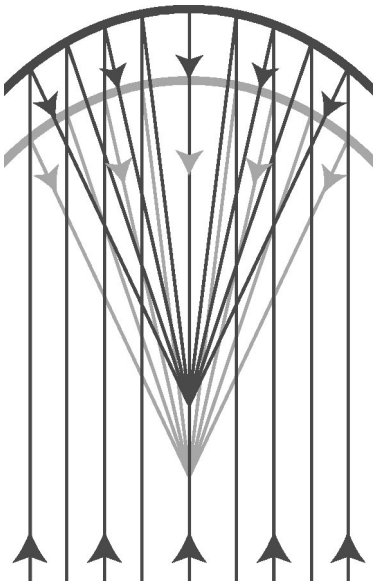

Fig. 10 A parabolic reflector perfectly focuses a collimated beam. When the reflector is coated with a ML, each transition between layers leads to a focus displaced by the equivalent distance in vacuum between the layer transitions. We assume that the refractive indices of the ML materials are close to unity.

The transitions in the ML lead to a summation of displaced foci. The relative contribution of each transition is given by Eq. (8). When using nongraded MLs, consisting of materials with a refractive index close to unity of which the thickness along the optical axis is constant, the axial shift between the different foci equals the thickness of a layer. Due to high absorption in the materials at EUV wavelengths, the contributions of the transitions further away from the top of the ML rapidly decrease. This decrease causes the asymmetry of the point spread function

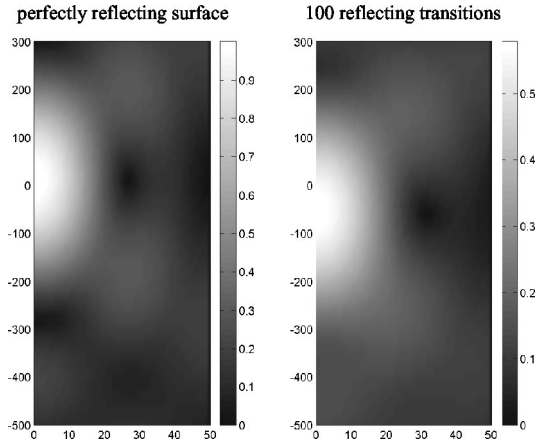

Fig. 11 The intensity of the point spread function of a perfect reflector with a numerical aperture of 0.3 in the image plane with a graded (left-hand side) and nongraded (right-hand side) ML of 50 periods. The axial defocus is plotted along the vertical axis, in a range from −500 to 300 nm. The radial distance r to the optical axis is plotted along the horizontal axis, in a range from 0 to 50 nm. The optical axis coincides with $r = 0$. Note the difference in grayscale between the two figures.

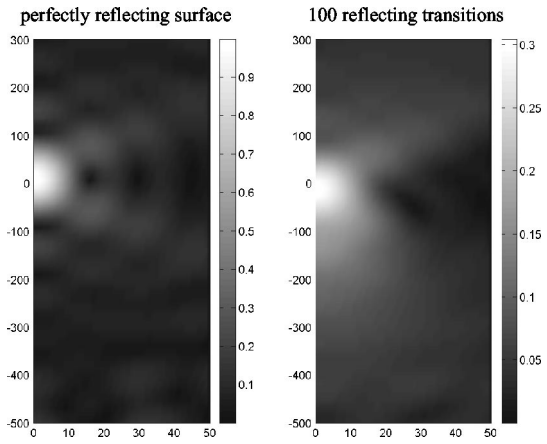

Fig. 12 The intensity of the point spread function of a perfect reflector with a numerical aperture of 0.5 in the image plane with a graded (left-hand side) or nongraded (right-hand side) ML of 50 periods. The ranges along the horizontal and vertical axis are the same as in Fig. 11.

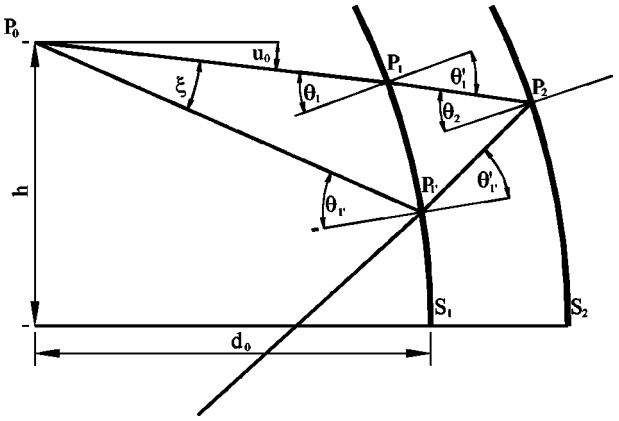

Fig. 13 The distributed reflection on a surface with a set of rays coming from an object in the top left of the picture. We adapt the shape of the layer $S2$ in such a way that the rays reflected by transition S_1 (ray P_0P_1') coincide with rays reflected at the second transition S_2 (ray $P_0P_2P_1'$).

when a ML is deposited on a reflector, as shown on the right-hand side of Fig. 11.

In Fig. 11, the numerical aperture in the image plane is 0.3, a target value for six-mirror EUV projection systems. The numerical aperture of eight-mirror systems is in the order of 0.4. To enhance the influence of the ML, we calculated the response of a system with a single ML with a numerical aperture of 0.5. In Fig. 12, we show the intensity of the point spread function. Here again, for comparison, the left-hand side shows the intensity of the point spread function of a parabolic mirror with a single reflective surface. The right-hand side shows the intensity of the point spread function in case the mirror is a ML with 50 periods.

In the case of the perfect mirror with a single reflective surface, the point spread function at a numerical aperture of 0.5 shows the 1/NA dependence of the feature size, as compared to an aperture of 0.3. The depth of focus depends approximately on the inverse square of the numerical aperture. With a ML instead of a single reflecting surface, the depth of focus increases, the feature size increases, and the reflectivity decreases. The main conclusion is that the incorporation of nongraded MLs severely degrades the optical performance. The thickness of the layers in the ML should be optimized to make the different foci coincide. In a graded ML, the thicknesses change as a function of the location on the mirror or, if preferred, as a function of the incidence angle [see Eq. (11)] to minimize the degradation of the point spread function.

4 Modeling of Graded Multilayers

The thickness l_j of the layers is normally in the order of a quarter wavelength and is adjusted for obliquely incident waves. A conventional method to calculate the grading of a ML is to evaluate the average (and the standard deviation) of the angles of incidence in a set of different positions on a surface. With the average of the angle of incidence θ, the rescaling factor of the thicknesses at a general position can be computed

$$l_j = \frac{\lambda}{4\,\mathrm{Re}[n_j]\cos\theta}, \tag{11}$$

where n_j is the complex refractive index of layer j. The rescaling factor only depends on the radial distance r to the optical axis, to retain the rotational symmetry in the system. As mentioned earlier, thin-film calculations coherently sum all reflections coming from the different transitions in the MLs, and assume an infinitely extending plane wave incident on a ML consisting of plane parallel surfaces. A condition that is better suited to our problem requires that the foci of all fields originating from different transitions coincide to achieve good optical imaging performance in the presence of a ML. The latter condition requires that all reflected fields generated by an incident ray be codirectional. We propose to use this condition to calculate the grading of MLs.

The condition that the different foci of the reflected fields of a single object point should coincide in the image plane implies that the propagation direction of rays on each position on the mirror is unique. This is the case for a reflecting surface with a single transition. In the case of MLs, an important benefit of our condition is that it becomes unnecessary to evaluate a set of rays per location on the surface. In the typical case of a Mo/Si EUV multilayer, this comprises at least a hundred different rays with different directions, intensities, origins, and phase shifts for each position on the ML surface. In Fig. 13, two rays originate from an object point P_0 located in the top-left corner of the picture at a height h and at an axial distance d_0 to the first reflective surface. The thick lines in Fig. 13 represent two near-conformal surfaces S_1 and S_2. Two rays originate from the object and hit the first surface. Of the first ray, we only consider the transmitted ray that is reflected on the second surface in point P_2. Of the second ray, we consider the reflected ray at the first surface at point $P_{1'}$. The angle of the first ray relative to the optical axis at the object point is u_0. For this ray, using Snel's law, we find,

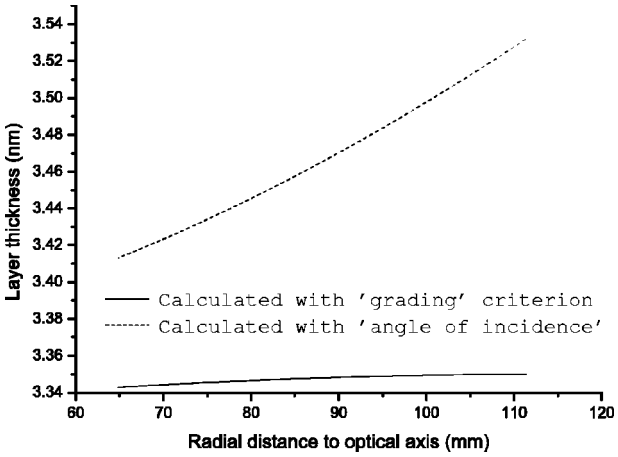

Fig. 14 The thickness of a single layer of Si on the first reflective surface of a four-mirror design, calculated with two methods. By the first method, we calculate the thickness of the ML as a function of the average cosine of the angle of incidence [see Eq. (11)]. The second method is the more rigorous method discussed in this work.

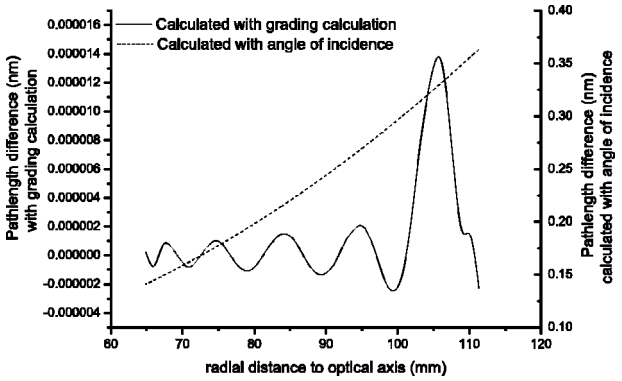

Fig. 15 The intended difference in the path length between a ray reflected at the first transition, and the second transition is half a wavelength. The difference between the intended and the actual path length difference is shown as a function of the radial distance to the optical axis. Note the extremely different vertical axis scales in the figure.

$$n_0 \sin(\theta_1) = \sin(u_0 + \alpha_1) = n_1 \sin(u_1 + \alpha_1) = n_1 \sin(\theta_1'), \tag{12}$$

where α_i is the slope of a surface in point P_i relative to the optical axis, and n_i is the refractive index of the material after surface i. The slope in an intersection point is given by

$$\alpha_i = \tan^{-1}\left(\frac{\partial z_i}{\partial r}\right)_{r=r_i}, \tag{13}$$

where z_i is the sag of surface I at the point P_i. The angle of the second ray is u_0 plus a small deviation ξ in the object space

$$\theta_2 = u_0 + \xi + \alpha_2, \tag{14}$$

$$n_0 \sin(u_0 + \xi + \alpha_{1'}) = -n_1 \sin(u_{1'} - \alpha_{1'}). \tag{15}$$

In Fig. 13, the intersection of the first ray with the second surface is at point P_2. The slope of the second mirror at point P_2 is given by

$$\alpha_2 = -\frac{u_1 + u_{1'}}{2}. \tag{16}$$

The deviation ξ should be such that the first and second ray both pass through the point $P_{1'}$ and propagate in the same direction. To get maximum enhancement, the phase difference between the two rays in point $P_{1'}$ should be a multiple of 2π.

The angle ξ is in general very small and can be found for a known object distance, object height, first surface position, and angle u_0. With the angle ξ, the position and slope of the point P_2 on the second surface is found. By varying the angle u_0 within the proper domain, a set of locations and slopes of the second reflective surface is found. These points and slopes of the surface can be simultaneously fitted to yield a polynomial expansion of the second surface. The results of the calculation of the grading of a layer are shown in Figs. 14 and 15. The further surfaces of the multilayers are calculated in a comparable way.

5 Conclusions

Common methods employed in thin-film calculations coherently sum all amplitudes reflected at the transitions in a ML. In the case of stratified planar ML structures with parallel interfaces, the superposition of the infinite series of reflected (or transmitted) waves can be represented by a single field. This field relates to the input field by an absolute relative amplitude and a phase-modulo 2π [see Eq. (1)]. In optical design using MLs, the layers can be replaced by a single effectively reflecting surface located at a certain depth. The absolute phase or the related effective depth of reflection can be determined by several methods discussed in this work. The most stable method calculates a weighted average of the depth of all interfaces. In a typical EUV ML consisting of 50 periods of Mo and Si, the effective reflection occurs at approximately 50 nm below the top of the ML. When including MLs in optical design programs, the positioning of the effective depth of reflection of a ML at the position of the original single transition engenders the smallest difference in optical characteristics of the system. The MLs and wavefronts in an EUV projection system are not flat. When MLs with uniform thicknesses of the different layers are used, the point spread function degrades. A conventional method to adjust the thicknesses of the layers uses the average cosine of the angle of incidence for thickness matching. We present a method that demands that the propagation direction of rays at a general position on a mirror must be unique, and that the difference in phase between all these rays equals an integer value of 2π. We have demonstrate the image improvement when using the latter method.

Acknowledgment

The authors thank ASM Lithography for supporting this research.

References

1. R. H. Stulen and D. W. Sweeney, ''Extreme ultraviolet lithography,'' *IEEE J. Quantum Electron.* **35**, 694–699 (1999).
2. E. Spiller, *Soft X-Ray Optics*, Chap. 8, SPIE Optical Engineering Press, Bellingham, WA (1994).
3. S. Bajt, J. B. Alameda, T. W. Barbee, W. M. Clift, J. A. Folta, B. Kaufmann, and E. A. Spiller, ''Improved reflectance and stability of Mo-Si multilayers,'' *Opt. Eng.* **41**(8), 1797–1804 (2002).
4. OSLO, Lambda Research Corporation, Littleton (2002).
5. Code V, Optical Research Associates, Pasadena, CA (2002).
6. C. Liang, M. R. Descour, J. M. Sasian, and S. A. Lerner, ''Multilayer-coating-induced aberrations in extreme-ultraviolet lithography optics,'' *Appl. Opt.* **40**, 129–135 (2001).
7. N. J. Duddles, ''Effects of Mo/Si multilayer coatings on the imaging characteristics of an extreme-ultraviolet lithography system,'' *Appl. Opt.* **37**, 3533–3538 (1998).
8. F. Cerrina, S. Bollepalli, M. Khan, H. Solak, W. Li, and D. He, ''Image formation in EUV lithography: Multilayer and resist properties,'' *Microelectron. Eng.* **53**, 13–20 (2000).
9. H. A. Macleod, *Thin-Film Optical Filters*, 2nd ed., pp. 11–43, Adam Hilger, Bristol, UK (1986).
10. TFCalc, Software Spectra Inc., Portland, OR (1999).
11. Y. Suematsu, S. Arai, and K. Kishino, ''Dynamic single-mode semiconductor lasers with a distributed reflector,'' *J. Lightwave Technol.* **LT-1**, 161–176 (1983).
12. L. R. Brovelli and U. Keller, ''Simple analytical expressions for the reflectivity and the penetration depth of a Bragg mirror between arbitrary media,'' *Opt. Commun.* **116**, 343–350 (1995).
13. M. Singh, M. F. Bal, and J. J. M. Braat, ''Wave-front correction methods for extreme-ultraviolet multilayer reflectors,'' *Appl. Opt.* **42**, 1847–1851 (2003).